

Modelling primary and secondary growth processes in plants: a summary of the methodology and new data from an early lignophyte

Thomas Speck^{1*} and Nick P. Rowe²

¹Plant Biomechanics Group, Institut für Biologie 2 und Botanischer Garten, Universität Freiburg, Schänzlestrasse 1, D-79104 Freiburg, Germany

²Botanique et Bioinformatique, AMAP, TA 40/PS2, Boulevard de la Lironde, F-34398 Montpellier Cedex 5, France

A mathematical method, based on polar coordinates that allow modelling of primary and secondary growth processes in stems of extant and fossil plants, is summarized and its potential is discussed in comparison with numerical methods using digitizing tablets or electronic image analysing systems. As an example, the modelling of tissue distribution in the internode of an extant sphenopsid (*Equisetum hyemale*) is presented. In the second half of the paper we present new data of a functional analysis of stem structure and biomechanics of the early lignophyte *Tetraxylopteris schmidtii* (Middle Devonian) using the polar coordinate method for modelling the tissue distribution in stems of different ontogenetic age. Calculations of the mechanical properties of the stems, based on the modelling of the tissue arrangement, indicate that there is no increase in structural bending modulus throughout the entire development of the plant. The oldest ontogenetic stage has a significantly smaller bending elastic modulus than the intermediate ontogenetic stage, a 'mechanical signal', which is not consistent with a self-supporting growth form. These results, and the ontogenetic variations of the contributions of different stem tissues to the flexural stiffness of the entire stem, are discussed in the evolutionary context of cambial secondary growth.

Keywords: functional anatomy; polar coordinates; biomechanics; growth form; *Equisetum hyemale*; *Tetraxylopteris schmidtii*

1. INTRODUCTION

Many woody plants show considerable changes in stem dimensions during ontogeny. In trees, for example, a young seedling with a length of several centimetres and a diameter of a few millimetres can grow to a huge tree with stem heights reaching, in some species, more than 100 m and diameters at breast height of 5 m or more (e.g. *Eucalyptus globulus*, h_{\max} : 120 m, d_{\max} : 8 m; *Pseudotsuga menziesii*, h_{\max} : 100 m, d_{\max} : 4.5 m; *Sequoiadendron giganteum*, h_{\max} : 120 m, d_{\max} : 11 m; Speck & Schmitt 1992). This increase in height and diameter is accompanied by marked variations in stem anatomy and dramatic changes in the contributions of different stem tissues towards the cross-sectional area and axial second moment of area. The contribution of the secondary wood increases considerably during ontogeny, whereas the contributions of cortex (used here for all tissues outside of the cambium) and pith significantly decrease. Contributions of wood towards the axial second moment of area, a geometrical value critical in bending mechanics, in hard- and softwood trees may increase from 10% or 20% (typically found in 1-year-old stems) up to more than 95% in large old trees (cf. Speck 1994a; Brüchert *et al.* 1995, 2000; Gallenmüller *et al.* 1999; Hlavatsch *et al.* 2000). By con-

trast, the cross-sectional shape of the three main tissues of the stem—pith, wood and cortex—remains relatively constant during ontogeny, forming ellipses, circles or circular rings. This is entirely different in many lianescent plants, where the cross-sectional shape of different stem tissues can change significantly during ontogeny (figure 1) with complex tissue arrangements developing in older climbing stems (cf. Speck 1994a; Rowe & Speck 1996; Speck *et al.* 1996; Speck & Rowe 1999a). In both fossil and living herbaceous plants, very different stem structures exist (figure 2). These range from relatively simple anatomies such as in *Rhynia gwynne-vaughanii* (Lower Devonian) to complex tissue arrangements such as those found in *Arachnoxylon kopfii* (Middle Devonian) and in the extant *Equisetum giganteum* and *Psilotum nudum*. The contribution of different stem tissues towards the cross-sectional area and axial second moment of area may also change during primary growth processes as can the cross-sectional shape of the stem tissues. With the exception of asymmetrical or bilaterally symmetrical stems caused, for example, by stem inclination or the influence of prevailing wind loads, most plant stems and the tissues comprising them are essentially centrisymmetrical in cross-section. This allows descriptions of the cross-sectional form of stems and stem tissues quantitatively with relatively simple mathematical procedures using polar coordinates. These formulae can also be used for calculating the cross-sectional areas and the polar and axial second moments of area of the different stem tissues and to model the

* Author for correspondence (thomas.speck@biologie-uni-freiburg.de).

One contribution of 20 to a Theme Issue 'Modelling in biomechanics'.

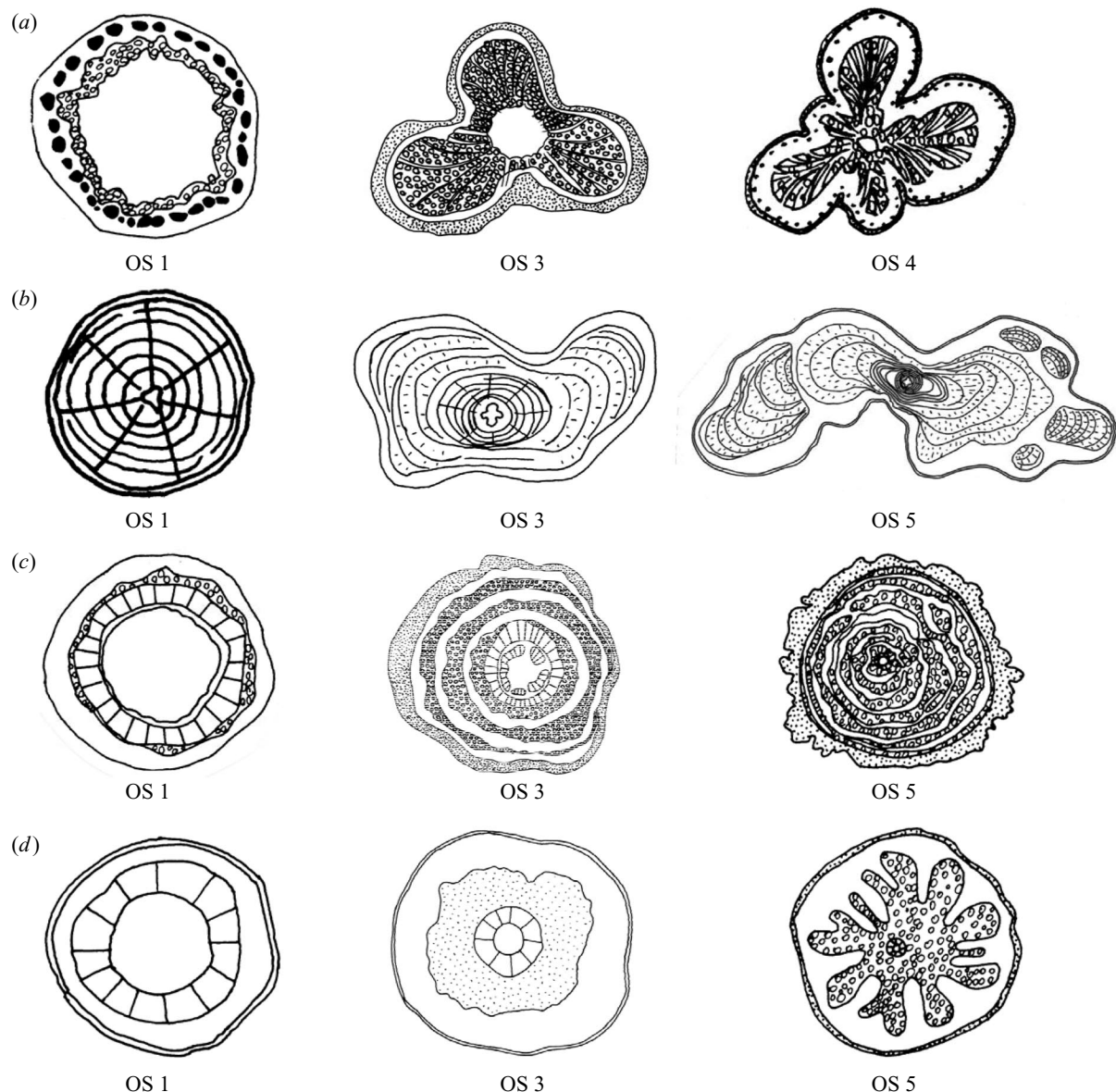


Figure 1. Ontogenetic variation in the cross-sections of four tropical lianas showing the pronounced structural variety found in stems of plants with a non self-supporting, lianescent growth habit: (a) *Passiflora glandulifera*; (b) *Bauhinia guianensis* agg.; (c) *Maripa scandens*; (d) *Condylocarpon guianense*. Tissues from the centre outwards: pith (central white area); dense wood (hatched area); less dense, lianescent wood (area marked with dashes and small circles representing large vessels); parenchymatous inner cortex, phloem and wood rays (white areas); sclerenchymatous tissues (black areas); outer cortex and bark (stippled area). Ontogenetic stage 1 (OS 1) includes cross-sections of young stiff searching axes, ontogenetic stage 3 (OS 3) shows medium-sized already relatively compliant stem parts, and ontogenetic stage 4/5 (OS 4/OS 5) old basal stem parts which are very flexible. (Modified from Speck *et al.* (1996) and Speck & Rowe (1999a), with permission.)

anatomical changes occurring in plants during primary and secondary growth. We summarize this approach, which has been published previously in a more theoretical manner (Speck *et al.* 1990) and discuss some new ideas on the advantages and disadvantages of this method when applied to extant and fossil plants. We present new results of the modelling of secondary growth processes and their influence on biomechanical stem properties in the early lignophyte *Tetraxylopteris schmidtii* (Middle Devonian), which is currently believed to be one of the earliest members of the lignophyte-clade to which the 'progymnosperms' (Aneurophytales, Archaeopteridales) and all seed plants (Spermatophyta) belong (Rothwell & Serbet 1994; Kenrick & Crane 1997; Rowe & Speck 2003).

2. METHOD FOR MODELLING COMPLEX CENTRISYMMETRIC STRUCTURES

Many plant tissues have a cross-sectional shape that can be modelled in good approximation with a star-shaped or lobed outline, as can be seen, for example, in *Maripa scandens* (figure 1c), *Condylocarpon guianense* (figure 1d), *A. kopfii* (figure 2b), *E. giganteum* (figure 2c) and *P. nudum* (figure 2d). We introduce a method using polar coordinates for modelling complex centrisymmetric structures with examples of star-shaped cross-sections.

(a) *Star-shaped cross-sections*

The outline of a star-shaped cross-section is generated in polar coordinates by defining a radius $r(\varphi)$ whose length

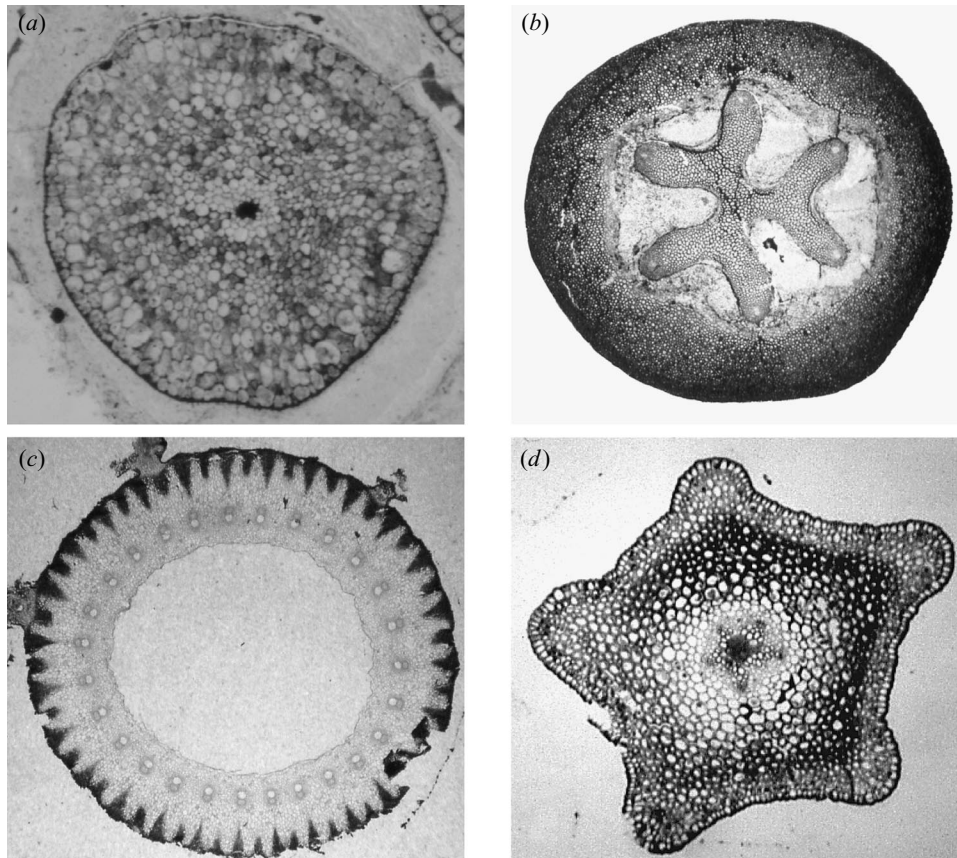


Figure 2. Tissue arrangements in cross-sections of fossil and extant herbaceous plants. (a) *Rhynia gwynne-vaughanii* (Early Devonian), showing a simple anatomy with tissues arranged in circles and circular rings; (b) *Arachnoxylon kopfii* (Middle Devonian) having a complex star-shaped stelar structure (from Taylor & Taylor 1993); (c) *Equisetum giganteum* (extant) internode with complex tissue arrangement (from Spatz *et al.* 1998a); (d) *Psilotum nudum* (extant) stem with star-shaped circumference, the outline of the sclerenchymatous cortex and the stele is also star-shaped (from Speck & Vogellehner 1994).

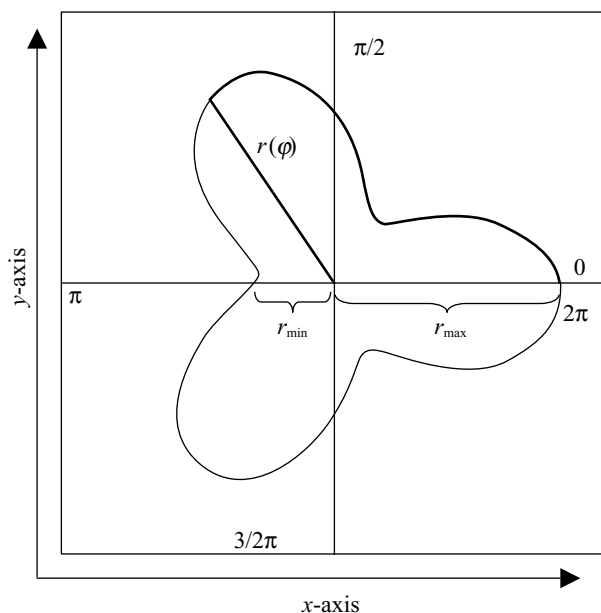


Figure 3. Star-shaped structure with three arms ($k=3$) and a relative extension of the arms of $\Psi=0.5$ modelled by using polar coordinates.

is defined by the following equation depending on the angle φ (cf. Baule 1979; Bronstein & Semendjajew 1981).

$$r(\varphi) = \frac{r_{\max}}{1 + \Psi} (1 + \Psi \cos k\varphi) = q(1 + \Psi \cos k\varphi). \quad (2.1)$$

The number of arms of the structure is given by k and their relative extension by Ψ , with

$$0 \leq \Psi = \frac{r_{\max} - r_{\min}}{r_{\max} + r_{\min}} \leq 1 \text{ and } q = \frac{r_{\max}}{1 + \Psi}. \quad (2.2)$$

The radius $r(\varphi)$ moves in a counter-clockwise direction from 0 to 2π and describes the outline of a star-shaped cross-section with a minimum radius r_{\min} and a maximum radius r_{\max} (figure 3). Double integration from 0 to $r(\varphi)$ and from 0 to 2π allows the calculation of the cross-sectional area A and the polar second moment of area I_p of the star-shaped formation, by using the basic formulae for A and I_p as given in engineering and biomechanics textbooks (e.g. Stephens 1970; Young 1989; Niklas 1992).

$$A = \int_0^{2\pi} \int_0^{r(\varphi)} r' dr' d\varphi = \pi q^2 (1 + 0.5\Psi^2) \quad (2.3)$$

$$I_p = \int r^2 dA = \int_0^{2\pi} \int_0^{r(\varphi)} r'^3 dr' d\varphi = 0.5\pi q^4 (1 + 3\Psi^2 + 0.375\Psi^4). \quad (2.4)$$

For centrisymmetric structures it is easier to calculate the polar second moment of area I_p that takes into consideration the cross-sectional area and cross-sectional shape of

a stem tissue by weighing the distribution of the area to the centre of mass (i.e. the neutral fibre) of the structure. The polar second moment of area is the tangible geometrical value as far as torsional loads are concerned. For two perpendicular axes through the centre of mass of the structure, as given by the x, y -coordinate system having its origin in the centre of mass of the structure

$$I_p = \int r^2 dA = I_x + I_y. \quad (2.5)$$

I_x and I_y are the axial second moments of area relative to the x -axis as neutral axis (I_x) or to the y -axis as neutral axis (I_y), respectively. For centrisymmetric structures with threefold symmetries or higher, i.e. in the case of star-shaped cross-sections for three or more arms ($k \geq 3$), it can be proved that for all neutral axes running through the centre of mass the axial second moment of area I_a is constant

$$I_a = I_x = I_y = 0.5I_p = 0.25\pi q^4(1 + 3\Psi^2 + 0.375\Psi^4). \quad (2.6)$$

It is interesting, that the cross-sectional area and the axial second moments of area are independent from the number of arms (k) of the star-shaped cross-section, and only depend on the maximum radius (r_{max}) and the relative extension of the arms (Ψ) (figure 4a,b). For a mathematically more detailed derivation of the formulae, discussions as to the bending efficiency of star-shaped formations with various outlines, and for a generalization of this approach by using Fourier series we refer to Speck *et al.* (1990).

(b) Central circles

Central circles can be considered as special cases of star-shaped cross-sections where the number of arms $k = 0$.

For $k = 0 \Rightarrow r(\varphi) = \text{const.} = r_{max} = r \Rightarrow \Psi = 0$ and $q = r$. (2.7)

With these variables, the above formulae for cross-sectional area A , polar second moment of area I_p and axial second moment of area I_a simplify to the well-known formulae for circles:

$$A = \pi r^2 \quad I_p = 0.5\pi r^4 \quad I_a = I_x = I_y = 0.25\pi r^4. \quad (2.8)$$

The combined axial second moments of area of complex structures such as circular rings, star-shaped circular rings and segmented rings can therefore be simply calculated by summation or subtraction of the axial second moments of area of simple structures (see Appendix A).

(c) Circles arranged in a single ring

Such an arrangement is also often found in cross-sections of plant tissues such as in eustelic vascular bundles or in the structure of vallicular and carinal canals in sphenopsids (horsetails) (figure 2c). To allow a mathematical treatment of this cross-sectional shape several conditions have to be fulfilled, and chosen to correspond as closely as possible with biological reality (figure 5):

- (i) the radii of the n small circles are constant: $r_s = \text{const.}$;
- (ii) the n small circles do not overlap.

If this holds, the cross-sectional area A trivially calculates as:

$$A = n\pi r_s^2. \quad (2.9)$$

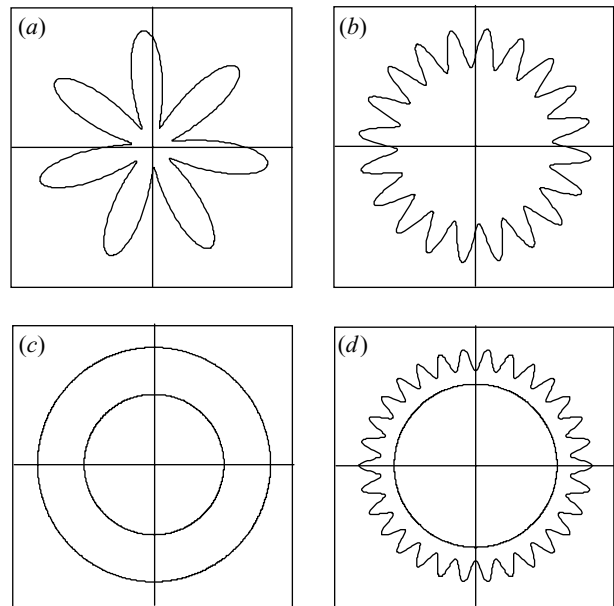


Figure 4. Examples for star-shaped cross-sections, circular rings and star-shaped rings. (a,b) Star-shaped cross-sections with $r_{max} = 1.0, k = 7, \Psi = 0.7$ and $k = 20, \Psi = 0.2$, respectively; (c) circular ring with $r_{max} = 1.0$ and $r_{min} = 0.6$; (d) star-shaped ring with $r_{max} = 1.0, k = 30, \Psi = 0.1$ (star-shaped outline), $r_{min} = 0.7$ (circular inner margin).

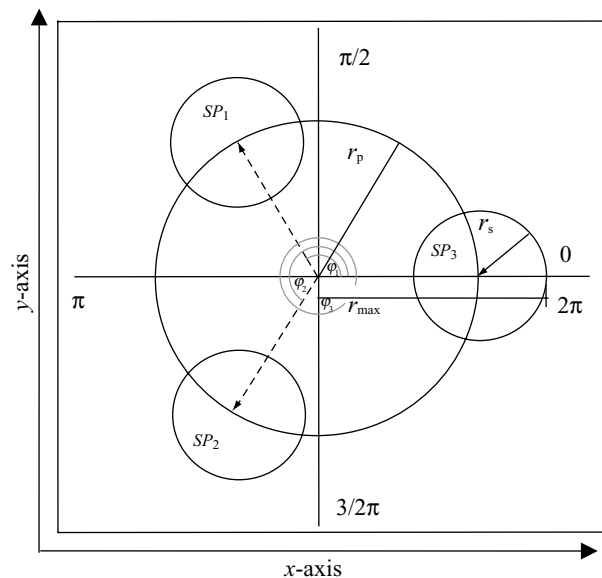


Figure 5. Circles arranged in a single ring. Three circles with a constant radius r_s are symmetrically arranged in a single ring with the radius r_p ; SP_1, SP_2, SP_3 are the centres of mass of the three small circles, $r_{max} = r_s + r_p$ (modified from Speck *et al.* 1990).

For finding a simple analytical solution for polar and axial second moments of area three additional conditions (again in good accordance with biological reality) have to be matched (Speck *et al.* 1990):

- (i) $SP_1, SP_2, SP_3, \dots, SP_n$ the centres of mass of the n small circles are arranged on a single circle with the radius: r_p ;
- (ii) the n small circles are symmetrically arranged
$$\varphi_i = 2\pi i/n \quad i = 1, 2, 3, \dots, n; \quad (2.10)$$

- (iii) the entire structure with a centre of mass in the origin of the x,y -coordinate system is centrisymmetric with a threefold symmetry or higher ($n \geq 3$).

For these conditions it can be proved that for all neutral axes running through the centre of mass the axial second moment of area I_a is constant:

$$I_a = I_x = I_y = 0.5I_p = 0.5\pi n(0.5r_s^4 + r_s^2r_p^2). \quad (2.11)$$

By summation the axial second moments of area of polycyclic structures, i.e. circles arranged on several concentric circles, can be calculated (see Appendix B).

3. TISSUE ARRANGEMENT IN *EQUISETUM HYEMALE* (SPHENOPSIDA, EQUISETACEAE)

As a first example we include an analysis of a species of horsetail (*Equisetum hyemale*), an extant sphenopsid. The method described above is used for modelling the geometrical arrangement of complex tissue structures in an internode and for calculating the contribution of the various tissues towards the cross-sectional area and axial second moment of area (figure 6).

For modelling the cross-sectional shape of the various stem tissues the outline of each respective tissue is described as follows:

- (i) outline of the stem: star-shaped formation with $r_{\max} = 1.000$, $k = 20$, $q = 0.982$, $\Psi = 0.018$;
- (ii) inner margin of the collenchymatous hypodermal sterome: star-shaped formation alternating with shallow and deep indentations with $r_{\max} = 0.945$, $k = 40$, $q_{\text{deep}} = 0.879$, $\Psi_{\text{deep}} = 0.075$, $q_{\text{shallow}} = 0.929$, $\Psi_{\text{shallow}} = 0.017$; the collenchymatous hypodermal sterome represents a star-shaped ring with a star-shaped outline (the outline of the stem) and a star-shaped inline (the outline of the parenchymatous tissue);
- (iii) vallecular canals: circles arranged on a single circle $n=20$, $r_p=0.774$, $r_s=0.079$;
- (iv) double endodermis including vascular bundles: circular ring plus circles arranged on a single circle $r_{\text{outer}} = 0.676$, $r_{\text{inner}} = 0.661$; $n = 20$, $r_p = 0.702$, $r_s = 0.018$;
- (v) pith cavity: central circle $r = 0.631$.

With this model the contribution of the stem tissues toward cross-sectional area and axial second moment of area can be calculated as follows.

tissue type	percentage cross-sectional area	percentage axial second moment of area
hypodermal sterome		
(collenchyma)	15.61	28.14
parenchymatous tissues	26.08	34.40
vallecular canals	14.27	17.79
double endodermis layer		
(including vascular bundles)	2.78	2.65
pith cavity	41.26	17.02

This example shows that even very complicated tissue arrangements such as internodes of extant and fossil sphenopsids (see Spatz *et al.* 1998a,b; Speck *et al.* 1998) can be modelled in good approximation. For a detailed discussion of the biomechanical properties and variation of the functional anatomy along the stem of *E. hyemale*, refer to Speck *et al.* (1998).

4. ADVANTAGES OF MATHEMATICAL MODELS BASED ON POLAR COORDINATES COMPARED WITH NUMERICAL ANALYSIS OF TISSUE DISTRIBUTION

This analysis of tissue distribution has several advantages over numerical methods involving digitizing tablets or image analysing systems.

- (i) When the mathematical model is formulated, only a few geometrical parameters need to be measured in stem cross-sections, making the method time efficient.
- (ii) Models allow predictions of how changes in tissue pattern during ontogeny or evolution will influence the mechanical properties of the stem. The role or function of specific tissues can therefore be assessed within evolutionary, ecological or developmental context and thus changes the mechanical importance of the different tissues can be assessed.
- (iii) If time-dependent formulae describing the various shapes of tissues were to be used, the dynamics of changes in tissue size and shape during ontogeny could be simulated, i.e. the plants could be 'grown artificially' in terms of their stem anatomy and mechanics.
- (iv) Cross-sectional area (A) and axial second moment of area (I_a) of different stem tissues can be modelled, and the mechanical significance of these tissues can be calculated even for fossil plant material often deformed during fossilization.
- (v) Hypothetical ontogenetic stages of a plant species missing in the fossil record can be modelled, and their mechanical properties can be quantitatively 'predicted'.

This modelling method for dealing with plant tissue geometries can be applied both for investigating mechanical and developmental trends in living plants and especially for modelling extinct plants that are preserved anatomically (see, for example, Speck & Vogellehner 1988, 1994; Rowe *et al.* 1993; Speck 1994b; Speck & Rowe 1994, 1999b, 2001; Rowe & Speck 1998, 2003; Niklas & Speck 2001). However, in living plant species with asymmetrical stem and tissue cross-sections or with very complicated tissue structures, numerical analyses may be preferable for a detailed functional analysis, as in recent studies of some *Clematis* species (see Isnard *et al.* 2003a,b).

5. FUNCTIONAL ANALYSIS OF *TETRARYLOPTERIS SCHMIDTII* (EARLY LIGNOPHYTE, MIDDLE DEVONIAN)

Anatomically preserved fossil plants offer the possibility of determining the geometrical distributions of tissues as

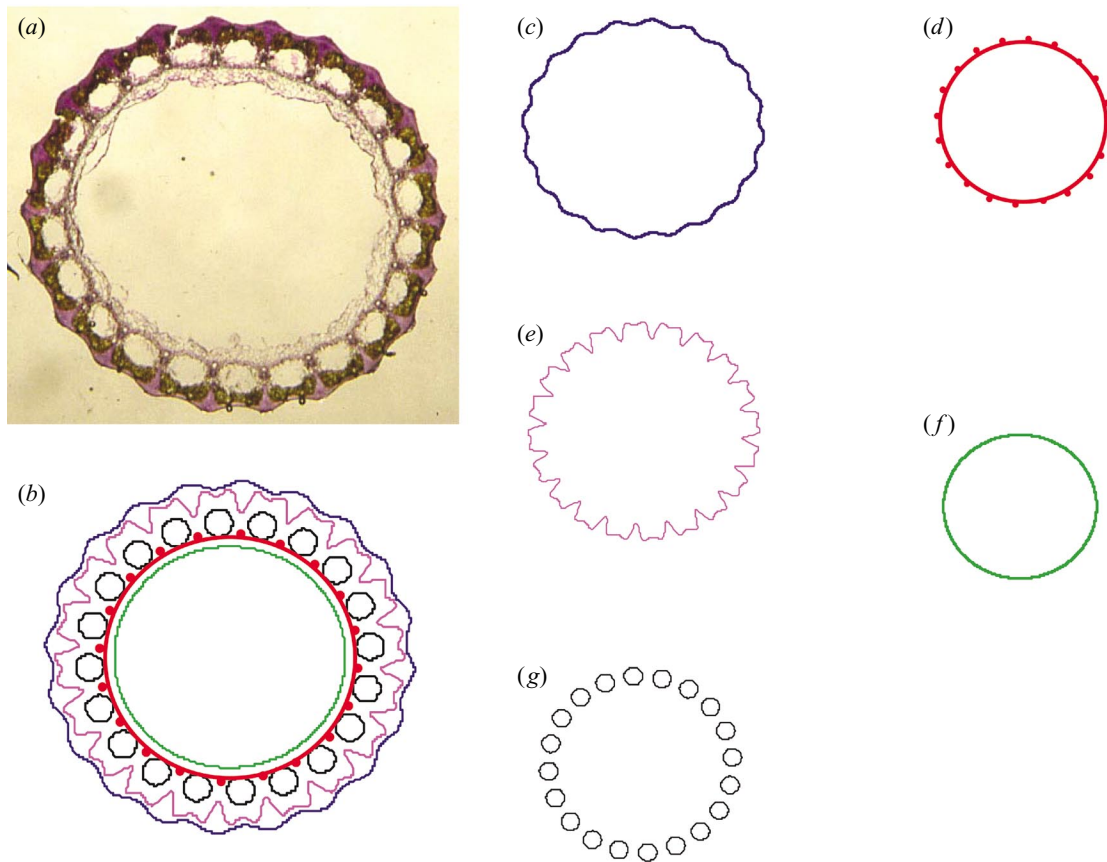


Figure 6. Tissue arrangement and polar coordinate models of an internode of *Equisetum hyemale*. (a,b) Cross-section through an internode of the middle part of the stem; (c) stem surface; (d) double endodermis and vascular bundles; (e) inner limit hypodermal sterome; (f) outer limit of pith cavity; (g) vallecular canals.

well as observing the cellular characteristics and cell wall thicknesses of individual cells (cf. Speck 1994b; Speck & Rowe 1999b). For most stem organizations, the component tissues can be approximated as centrisymmetric arrangements as outlined above. The principal step in producing a model based on fossilized plant material is to construct centrisymmetric models of the tissue distributions and calculate the contribution to the second moment of area of each tissue. The second step is to attribute values of bending elastic modulus to each fossil tissue. The latter is based on comparisons of cell shape, wall thickness and cell wall ornamentation of biomechanically tested living plant tissues (Speck & Rowe 1999b, 2001). Values of bending elastic modulus for specific fossil tissues ($E_{\text{tissue},i}$) are therefore based on values for the most similar tissues measured from living plants such as parenchyma, collenchyma, sclerenchyma, xylem tissue, bark tissue, wood and phloem. Values of bending elastic modulus can be modified according to variations in wall thickness or variations observed among living tissues in terms of cell shape.

$$E_{\text{struct}} = \left(\sum_{i=1}^m E_{\text{tissue},i} I_{\text{tissue},i} \right) / I_{\text{stem}}, \quad FS_{\text{struct}} = \sum_{i=1}^m E_{\text{tissue},i} I_{\text{tissue},i}, \quad (5.1)$$

$$FS_{\text{tissue},i} = E_{\text{tissue},i} I_{\text{tissue},i} / FS_{\text{struct}}. \quad (5.2)$$

- (i) E_{struct} : structural bending elastic modulus of the entire stem

- (ii) FS_{struct} : flexural stiffness of the entire stem
- (iii) $I_{\text{tissue},i}$: axial second moment of area of the i th fossil tissue
- (iv) $E_{\text{tissue},i}$: bending elastic modulus of the i th fossil tissue, calculated from values experimentally determined from living tissues
- (v) $FS_{\text{tissue},i}$: contribution of the i th fossil tissue towards the flexural stiffness of the stem
- (vi) I_{stem} : axial second moment of area of the entire fossil stem
- (vii) m : number of different stem tissues.

In this paper, we follow the terminology used in recent investigations where the term structural bending elastic modulus or structural Young's modulus is employed for this quantity in plant stems, which are clearly composite structures rather than homogeneous materials (Rowe & Speck 1996, 1998; Speck & Rowe 1999a; Gallenmüller *et al.* 2001).

Values of flexural stiffness are then calculated for each tissue ($FS_{\text{tissue},i} = E_{\text{tissue},i} I_{\text{tissue},i}$) and for the entire cross-sectional area of the stem. From the simple arithmetical relations between flexural stiffness, second moment of area and bending elastic modulus, the following parameters can be derived from the model which concern the mechanical properties and change in properties of the plant stem as a whole: the flexural stiffness (FS_{struct}) and structural bending elastic modulus of the entire stem (E_{struct}), and the contribution of each of the m tissues to

the flexural stiffness of the stem ($FS_{\text{tissue},i}$). To test the accuracy of this approach we have measured the bending mechanical properties of the stems of some extant plant species experimentally. We have then compared these experimental results with the values calculated by using independently measured bending elastic moduli of the different stem tissues and their respective contributions to the axial second moment of area. In all cases we found a very good agreement between calculated and experimentally measured data (Speck *et al.* 1996; Brüchert *et al.* 2000).

A key part of the analyses on fossil stems concerns the fact that mechanical parameters are calculated for different ontogenetic stages, as well as different sizes of stem and thus describe a 'signal' of how mechanical properties change between growth stages or branch levels of the plant. These data are directly comparable with recent studies on living plants in which biomechanical signals traced during development can readily distinguish different growth forms such as self-supporting trees and shrubs, semi-self-supporting plants, creeping plants, root climbers and lianas (cf. Speck 1994a; Speck & Rowe 1999a). For example, trends in parameters such as flexural stiffness and structural bending elastic modulus show different patterns between trees and lianas, and these can be compared with the trends observed for fossils. These composite models can also explore the 'performance' or contribution of specific tissues to the geometry and flexural stiffness of the stem. In an evolutionary context this presents an opportunity to investigate which tissue components were important for the bending stiffness of the stem at many stages of evolution from simple early land plants to sophisticated and complex organizations, including one or more types of secondary growth.

In the following section, we outline a new biomechanical analysis on one of the earliest known plants with secondary growth (Beck 1957; Scheckler 1976; Taylor & Taylor 1993; Niklas 1997). Recent phylogenetic studies place this plant and allied forms at the base of the lignophytes, a clade characterized by a secondary vascular cambium (Kenrick & Crane 1997). This structure is a sophisticated lateral meristem producing wood (secondary xylem and ray tissue) towards the inside and secondary phloem tissue towards the outside. The structure characterizes all lignophytes before the evolution of the seed as well as all seed plants. Some groups, most notably monocotyledons, have lost this type of secondary growth. The appearance of the combination of wood and secondary phloem possibly represented a key innovation that allowed wide-scale architectural and physiological radiations of plant growth forms (Rowe 2000; Rowe & Speck 2003). Wood is clearly an important mechanical element of many self-supporting and non-self-supporting plants. In the following mechanical analysis, we decided to investigate whether one of the earliest and phylogenetically basal lignophytes was a self-supporting growth form and to what extent the wood contributed towards a self-supporting growth form within the constraints of the developmental patterns and contributions from other tissues.

6. METHODS

Centrisymmetrical models of the *Tetraxylopteris* stem were constructed after observation of fossil slide preparations generously

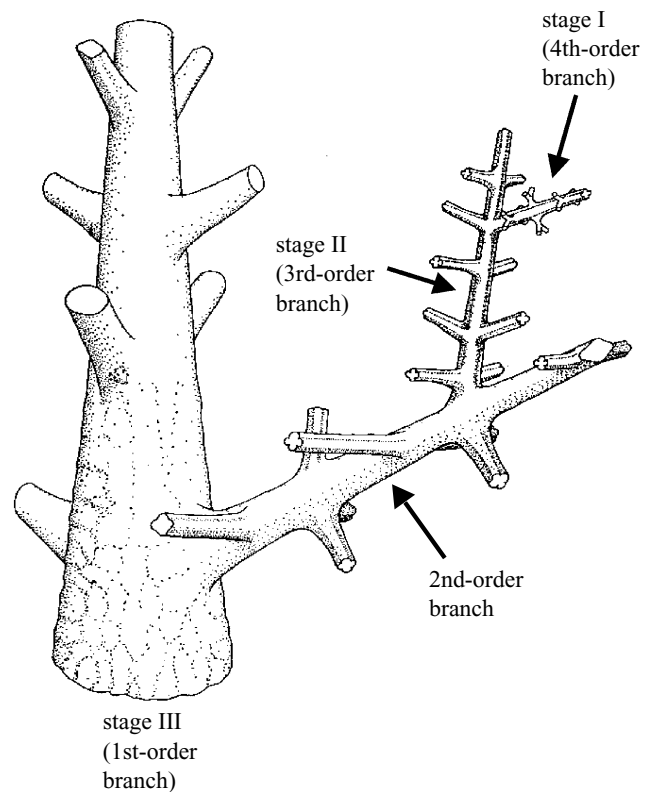


Figure 7. Schematic reconstruction of a branching system of *Tetraxylopteris schmidtii* (modified from S. Scheckler). Four branching orders are shown; from three of them (stage I, II and III) anatomically preserved material exists and is included in our analysis.

donated by Dr S. Scheckler. The material comes from the Middle Devonian of New York state and its cellular details are preserved by preservation in pyrite (Scheckler 1976). A previous description identified four developmental stages of this plant (figure 7) and in the available material sufficient anatomical preservation was present to construct three centrisymmetrical stages of development.

7. MODEL

The youngest stage (figure 8a,b) corresponds to a four-armed star-shaped outline with tissues from outside to inside represented by: (i) hypodermal sterome of alternating longitudinal bands of collenchyma fibres and parenchyma; (ii) cortical region of large parenchyma cells; (iii) narrow zone of a mixture of primary phloem and small amounts of secondary phloem; (iv) the stele area comprising primary xylem and pith as well as small amounts of secondary xylem.

The second stage (figure 8c,d) included significant levels of secondary growth. Tissues from outside to inside included: (i) hypodermal sterome of alternating bands of collenchyma fibres and parenchyma; (ii) narrow zone of collapsed parenchymatous cortex and secondary phloem; (iii) broad zone of secondary xylem and ray tissue (wood); (iv) primary xylem and pith of central stele.

The third and final stage (figure 8e,f) included, from outside to inside: (i) an outer bark-like tissue resulting from cellular proliferation of the secondary phloem; (ii) two oval to circular branch traces; (iii) a zone of secondary

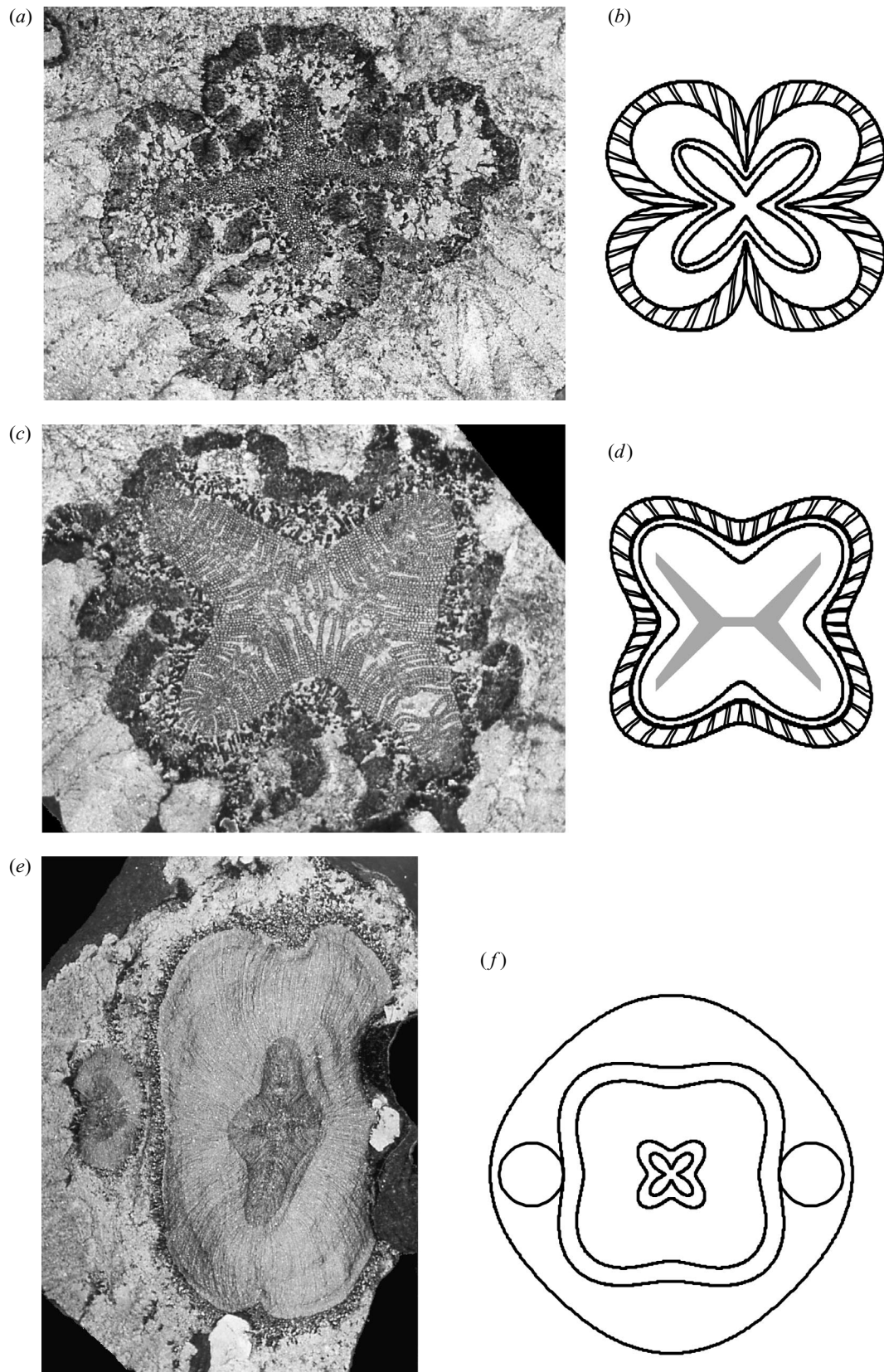


Figure 8. *Tetraxylopteris schmidtii*, cross-sections of stages of development and polar coordinate models of these cross-sections showing the arrangement of the different stem tissues. (a,b) Small fourth-order branch (youngest ontogenetic stage I) tissue types from outside to centre: hypodermal sterome, parenchymatous cortex, phloem, primary xylem; (c,d) medium-sized third-order branch (intermediate ontogenetic stage II) tissue types from outside to centre: hypodermal sterome, parenchymatous cortex, secondary phloem, secondary xylem, primary xylem; (e,f) old first-order branch (oldest ontogenetic stage III) tissue types from outside to centre: bark-like tissue, second-order branch trace, secondary phloem, outer secondary xylem, inner secondary xylem, primary xylem.

phloem; (iv and v) zones of dense outer and inner secondary xylem and ray tissue divided into four shallow differentiated arms; (vi) primary xylem.

8. ASSUMPTIONS

As in all attempts at modelling fossil organisms quantitatively a range of assumptions were necessary for either simplifying or combining complex elements that are not readily handled. Apart from the basic assumptions inherently involved in the bending theory of composites (cf. Wainwright *et al.* 1976; Speck *et al.* 1990; Niklas 1992; Vincent 1992) two main additional assumptions were necessary for the model of *Tetraxlopteris*. These concerned: (i) the mechanical properties in bending of the outer bark-like tissue of the periderm (figure 8*e, f*) which is not readily comparable with biomechanically tested modern barks; and (ii) the mechanical contribution of the two lateral branch traces (figure 8*e, f*) which are not longitudinally continuous along the stem but depart at relatively wide angles at the nodes. We decided to adopt an experimental approach similar to that carried out in a previous analysis modelling fossil twigs of the Carboniferous seed plant *Pitus dayi* (Speck & Rowe 1994). In this case we modified the basic composite model into a series of 'what if' scenarios or simulations with: (i) variable mechanical values of E_{str} for the periderm; and (ii) the construction of two basic models based on the nodal (= with branch traces) and internodal (= without branch traces) parts of the stem.

9. RESULTS

In the following section we discuss the findings based on the structural bending elastic modulus of the stem for each level of branching as well as the contribution of some of the main tissues towards flexural stiffness of the stem. For the results based on structural bending elastic modulus, we present alternative calculations for the oldest stage III in both the nodal and internodal parts of the stem. For reasons outlined below in the discussion, we present only data based on the internodal regions of the stem for the data based on contributions towards flexural stiffness.

(a) *Model I: periderm (bark) of oldest stage III modelled as a mixture of collenchyma fibres and parenchyma tissue*

The model based on the internodal region of the stem shows a pattern of values between young stems (stage I) and old stems (stage III) varying from 2700 to 2800 MPa, respectively with the intermediate stage II having a relatively higher value of 4400 MPa (figure 9*a*). The analysis of the nodal region in which two calculations are necessary to describe the bilaterally symmetrical structure, indicate a similar pattern in which the calculation for the oldest stage related to the y -axis as a neutral axis shows a slightly higher modulus influenced by the contribution of branch traces (figure 9*b*).

The data based on the contribution of each tissue to flexural stiffness in the internodal region indicate that the first two stages are dominated by the contribution of the outer fibre tissues, which contribute almost 90% of the

flexural stiffness in branches of stage I and nearly 50% in branches of stage II in which fibrous secondary phloem contributes another 10% (figure 9*c*). In this model the partly fibrous peridermal tissue contributes almost 50% and the fibrous secondary phloem over 15% of the flexural stiffness in old branches of stage III. Despite the relatively large volume of wood in stage I branches, its contribution to flexural stiffness of the stem is only just over 35%.

(b) *Model II: periderm (bark) of oldest stage III modelled as bark-like tissue*

The model based on the internodal region differs from model I in the value of the oldest stage III, which shows a structural bending elastic modulus of only 1700 MPa (figure 10*a*). During the development of the stem from young to old stages there is therefore an increase followed by a more marked decrease in the modulus of the stem. As in model I, the nodal distribution of the structural bending elastic modulus shows an elevated value where the branch traces are orientated further away from the neutral plane of bending along the y -axis (figure 10*b*).

The contribution of different tissues to flexural stiffness in the internodal region of the stem differs markedly from that in model I, with the bark-like peridermal tissue contributing less than 15% and the secondary xylem and the fibrous secondary phloem contributing *ca.* 60% and 25%, respectively (figure 10*c*).

(c) *Interpretation and comparison of models*

A comparison of the models above indicates that there is no increase of structural bending elastic modulus during the entire development of the plant from stage I to stage III. Compared with all tested living plants, this is not typical of self-supporting plants—plants that can remain upright without recourse to some sort of lateral support. This result holds true for all of the tested models, whether the periderm is modelled as a fibre and parenchymatous tissue or as a bark-like tissue. In the second model, stage III (periderm = bark-like tissue) shows a more marked drop in modulus compared with model I, with a modulus less than 50% of stage II. This pattern is not at all consistent with a self-supporting growth form.

The models including the branch traces (nodal models) in the calculations do not qualitatively change the pattern in structural bending elastic modulus during ontogeny. In neither case do the contributions of woody branch traces elevate the value of the structural bending elastic modulus in the older stages to values higher than those of stage II. Therefore, even taking into consideration the horizontal branch traces in the older stage of growth, the pattern in the structural bending elastic modulus is not that of a self-supporting plant. We favour an interpretation based on the internodal region of the stem. Branch traces will only locally stiffen portions of the stem as a whole whereas internodal regions represent the 'weaker' link in a longitudinally complex structure. We, therefore, prefer to take the internodal regions as the value dictating the probable bending properties and resistance to bending of the stem as a whole.

The contribution of tissues to the flexural stiffness of the stem clearly shows the transition from a hypodermal mechanical architecture to one in which secondary tissues

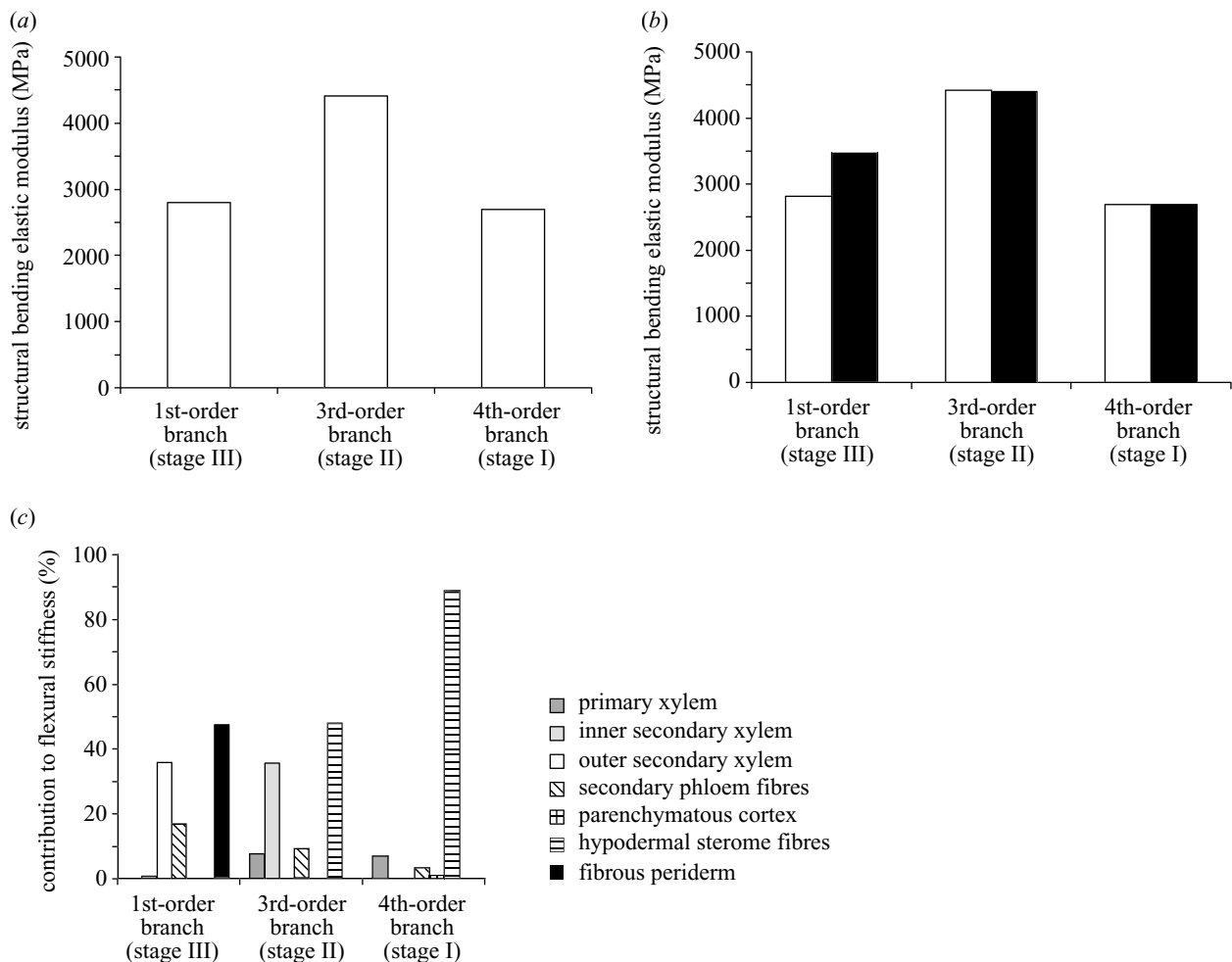


Figure 9. *Tetraxylopteris schmidtii*. (a,b) Variation of structural bending elastic modulus during ontogeny: model I—periderm (bark) of oldest stage III modelled as a mixture of collenchymatous fibres and parenchymatous tissue; (a) internodal region without branch traces in stage III branches; (b) nodal region with branch traces in stage III branches (I_y , y -axis as neutral line): filled bars; I_x (x -axis as neutral line): open bars); (c) percentage contribution of tissues towards flexural stiffness in the internodal region.

contribute to the mechanics of the stem. Younger axes are dominated by the outer primary fibre tissue, which is placed on the outside of the stem and is optimally positioned in terms of the second moment of area to resist bending forces. The first model incorporating a mixture of fibres and parenchyma indicates that the final stage of development has a mechanical architecture dominated by an outer mechanical periderm or bark. The second model indicates that if the outer periderm tissue is modelled as a mostly bark-like tissue, the contributions from the wood and the phloem are more significant and that the fibrous and more peripheral phloem tissue has a smaller contribution than the wood. Our preference is to favour results based on a parenchymatous tissue, rather than one in which fibres contribute significant stiffness to such a tissue. Close inspection of the fossil tissue indicates that fibres and thick-walled stone cells were scattered and probably did not confer any appreciable stiffness to the periderm tissue.

These results indicate that the growth form of *Tetraxylopteris* was not typical of self-supporting plants. The early stages of growth depended on an outer primary ring of mechanical tissue that provided a high level of stiffness. This is an organization characteristic of many other

contemporaneous architectures. The results indicate that *Tetraxylopteris* did indeed modify the primary body of the plant by secondary growth but that the older, possibly more basal stem had a lower structural bending modulus than the younger and more apical plant stems. This suggests that the appearance of wood in this species, and perhaps others, was not a mechanical feature that was optimized for producing a self-supporting growth form (Rowe & Speck 2003). The geometrical modelling of all tissues, as well as the comparison of models, indicate that even if the peridermal tissue is modelled as a fibrous tissue the oldest developed stage does not show a higher structural bending elastic modulus than the younger stage. This is also true whether we include the lateral branch traces as a 'nodal model' or disregard them as an 'internodal model'.

10. CONCLUSIONS

Modelling plant stems and their composite tissue surfaces through polar coordinates is a convenient method of constructing complex patterns that can approximate closely to biological organizations of primary and secondary tissues. Geometric analyses of living plants can be

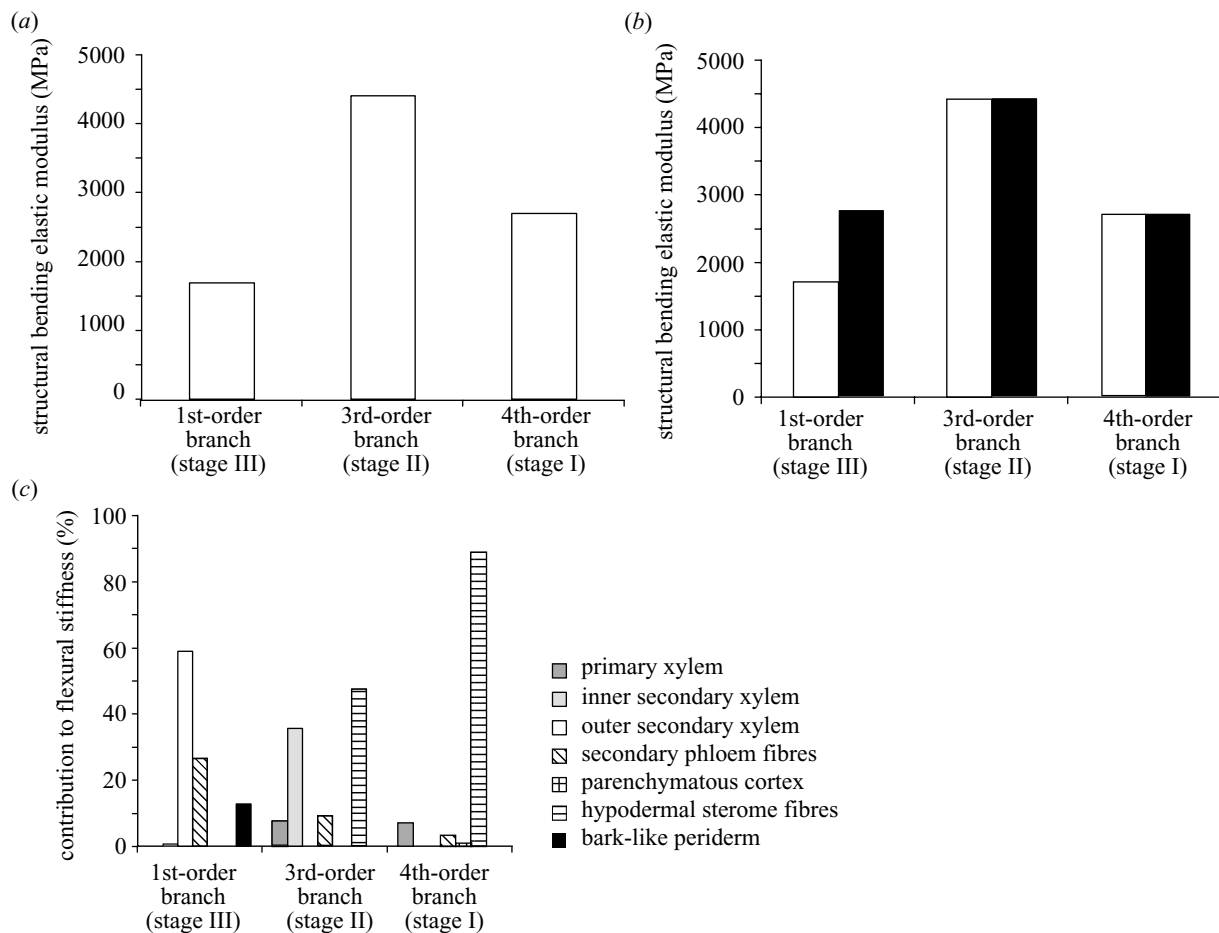


Figure 10. *Tetraxylopteris schmidtii*. (a,b) Variation of structural bending elastic modulus during ontogeny: model II—periderm (bark) of oldest stage III modelled as bark-like tissue; (a) internodal region without branch traces in stage III branches; (b) nodal region with branch traces in stage III branches (I_y , (y -axis as neutral line): filled bars; I_x (x -axis as neutral line): open bars); (c) percentage contribution of tissues towards flexural stiffness in the internodal region.

readily tested against digitized surfaces through images, and thus tested so that simple and relatively few centrisymmetric measurements can be used to generate complex models. Models of fossil tissues are particularly amenable to this simple method and are being used to investigate the growth form diversity and evolutionary significance of potential innovations such as the appearance of secondary growth in plants. The simple approach is also appropriate for testing alternative hypotheses and ‘bracketing’ mechanical values of fossil tissues that are difficult to interpret. The method can also be used for reciprocal hypothesis testing when exploring the evolution of plant growth forms. The plant growth form itself and the mechanical importance of individual tissues can be further tested when additional growth stages are found in the fossil record and can be added to the existing analysis to see whether the trend in structural bending elastic modulus significantly changes. Such flexibility in the approach is an excellent way of developing ideas as new data are found, and in the case of *Tetraxylopteris* will ultimately test whether the hypothesis stating that wood was not initially a mechanical innovation, stands or falls.

The authors thank Dr S. Scheckler who generously donated the slide preparations of *Tetraxylopteris schmidtii*. This study was done during the receipt of a PROCOPE award to T.S.

and N.P.R. (from DAAD and A.P.A.P.E.), which is gratefully acknowledged.

APPENDIX A: CIRCULAR RINGS, STAR-SHAPED CIRCULAR RINGS AND SEGMENTED STRUCTURES

For calculating the areas, polar and axial second moments of area of circular rings and star-shaped rings the additive or subtractive properties of areas and second moments of area are used, by simply subtracting the value of the inner cross-sectional structure from the value of the outer structure (figure 4c,d).

$$\begin{aligned} A_{\text{ring}} &= A_{\text{outer}} - A_{\text{inner}} \\ I_{p,\text{ring}} &= I_{p,\text{outer}} - I_{p,\text{inner}} \\ I_{a,\text{ring}} &= I_{a,\text{outer}} - I_{a,\text{inner}} \end{aligned} \quad (\text{A } 1)$$

The same holds for systems of several concentric, non-overlapping circular rings or star-shaped rings that can also be treated as superimposed of single concentric rings.

The additive or subtractive properties can also be used for calculating areas and second moments of area for segments of central circles, star-shaped formations or ring-like structures, if these segmented structures have a three-fold symmetry or higher (cf. Rowe *et al.* 1993; Speck & Rowe 1994).

APPENDIX B: CIRCLES ARRANGED IN SEVERAL CONCENTRIC RINGS

Polycyclic structures can be treated as a superimposition of monocyclic structures by taking advantage of the additive properties of cross-sectional areas and second moments of area. If, for each of the monocyclic subsystems, the above conditions are fulfilled and the circles of the different subsystems do not overlap, relatively simple analytical solutions for the polar and axial second moments of area are possible. In particular, this holds if the radii of the single circles are constant in the entire polycyclic structure, and if the number of single circles is either constant in each monocyclic subsystem or increases in a regular manner from the innermost to the outermost subsystem. The latter ($r_s = \text{constant}$ and a regularly increase from the innermost to the outermost cycle) can be used in good approximation for modelling the atactosteles of some monocotyledonous plants and the polysteles of some extant and fossil ferns and other fossil herbaceous plants.

The approach discussed above can be extended to all types of centrisymmetric structure, even if they have rather complex cross-sectional shapes as found, for example, in stelar systems of extant and fossil plants (Speck & Vogel-lehner 1988).

REFERENCES

- Baule, B. 1979 *Die Mathematik des Naturforschers und Ingenieurs (in 2 volumes)*. Thun-Frankfurt/M: Verlag Harry Deutsch.
- Beck, C. B. 1957 *Tetrazylopteris schmidtii* gen. et spec. nov., a probable pteridosperm precursor from the Devonian of New York. *Am. J. Bot.* **44**, 350–367.
- Bronstein, I. N. & Semendjajew, K. A. 1981 *Taschenbuch der Mathematik.*, 21st/22nd edn. Thun-Frankfurt/M: Verlag Harry Deutsch.
- Brüchert, F., Bogenrieder, A. & Speck, T. 1995 Biomechanisch-ökologische Untersuchungen an Sprossachsen von Schwarz-Erle und Grün-Erle. *Mitteil. badisch. Landesvereins Naturk. Natursch. N.F.* **16**, 389–396.
- Brüchert, F., Becker, G. & Speck, T. 2000 The mechanics of Norway spruce (*Picea abies* [L. (Karst)]): the mechanical properties of standing trees from different thinning regimes. *Forest Ecol. Mgmt* **135**, 45–62.
- Gallenmüller, F., Bogenrieder, A. & Speck, T. 1999 Biomechanische und ökologische Untersuchungen an *Alnus viridis* (Chaix) DC. in verschiedenen Höhenlagen der Schweizer Alpen. *Berichte Eidgenöss. Forschungs. Wald, Schnee Landschaft. WSL/FNP* **347**, 1–31.
- Gallenmüller, F., Müller, U., Rowe, N. P. & Speck, T. 2001 The growth form of *Croton pullei* (Euphorbiaceae) functional morphology and biomechanics of a neotropical liana. *Pl. Biol.* **3**, 50–61.
- Hlavatsch, S., Bogenrieder, A. & Speck, T. 2000 Funktionsanatomie und Biomechanik der Grau-Erle (*Alnus incana*): Vergleich von Pflanzen von unterschiedlichen Standorten im südlichen Schwarzwald. *Berichte Naturforsch. Gesellsch. Freiburg* **88/89**, 249–276.
- Isnard, S., Rowe, N. P. & Speck, T. 2003a Growth habit and mechanical architecture of the sand dune-adapted climber *Clematis flammula* var. *maritima* L. *Ann. Bot.* **91**, 407–417.
- Isnard, S., Speck, T. & Rowe, N. P. 2003b Mechanical architecture and development in *Clematis* L.: implications for canalised evolution of growth form. *New Phytol.* **158**, 543–559.
- Kenrick, P. & Crane, P. R. 1997 *The origin and early diversification of land plants: a cladistic study*. Washington, DC: Smithsonian Institution Press.
- Niklas, K. J. 1992 *Plant biomechanics*. University of Chicago Press.
- Niklas, K. J. 1997 *The evolutionary biology of plants*. University of Chicago Press.
- Niklas, K. J. & Speck, T. 2001 Evolutionary trends in safety factors against wind-induced stem failure. *Am. J. Bot.* **88**, 1266–1278.
- Rothwell, G. W. & Serbet, R. 1994 Lignophyte phylogeny and the evolution of spermatophytes: a numerical cladistic analysis. *Syst. Bot.* **19**, 443–482.
- Rowe, N. P. 2000 The insides and outsides of plants: the long and chequered evolution of secondary growth. In *Plant Biomechanics 2000, Proc. of the 3rd Int. Plant Biomechanics Conf.*, Badenweiler, Freiburg (ed. H.-Ch. Spatz & T. Speck), pp. 129–140. Stuttgart: Thieme-Verlag.
- Rowe, N. P. & Speck, T. 1996 Biomechanical characteristics of the ontogeny and growth habit of the tropical liana *Condylocarpon guianense* (Apocynaceae). *Int. J. Pl. Sci.* **157**, 406–417.
- Rowe, N. P. & Speck, T. 1998 Biomechanics of plant growth forms: the trouble with fossil plants. *Rev. Palaeobot. Palynol.* **102**, 43–62.
- Rowe, N. P. & Speck, T. 2003 Hydraulics and mechanics of plants: novelty, innovation and evolution. In *The evolution of plant physiology* (ed. A. R. Hemsley & I. Poole), pp. 301–329. London: Academic Press.
- Rowe, N. P., Speck, T. & Galtier, J. 1993 Biomechanical analysis of a Palaeozoic gymnosperm stem. *Proc. R. Soc. Lond. B* **252**, 19–28.
- Scheckler, S. E. 1976 Ontogeny of progymnosperms. I. Shoots of Upper Devonian Aneurophytales. *Can. J. Bot.* **54**, 202–219.
- Spatz, H.-C., Köhler, L. & Speck, T. 1998a Biomechanics and functional anatomy of hollow stemmed sphenopsids: I. *Equisetum giganteum*. *Am. J. Bot.* **85**, 305–314.
- Spatz, H.-C., Rowe, N. P., Speck, T. & Daviero, V. 1998b Biomechanics of hollow stemmed Sphenopsids. II. *Calamites*—to have or not to have secondary xylem. *Rev. Palaeobot. Palynol.* **102**, 63–77.
- Speck, T. 1994a Bending stability of plant stems: ontogenetical, ecological, and phylogenetical aspects. *Biomimetics* **2**, 109–128.
- Speck, T. 1994b A biomechanical method to distinguish between self-supporting and non self-supporting plants. *Rev. Palaeobot. Palynol.* **81**, 65–82.
- Speck, T. & Rowe, N. P. 1994 Biomechanical analysis of *Pitus dayi*: early seed plant vegetative morphology and its implications on growth habit. *J. Pl. Res.* **107**, 443–460.
- Speck, T. & Rowe, N. P. 1999a A quantitative approach for analytically defining size, form and habit in living and fossil plants. In *The evolution of plant architecture* (ed. M. H. Kurmann & A. R. Hemsley), pp. 447–479. Kew: Royal Botanic Gardens Kew.
- Speck, T. & Rowe, N. P. 1999b Biomechanical analysis. In *Fossil plants and spores: modern techniques* (ed. T. P. Jones & N. P. Rowe), pp. 105–109. London: Geological Society.
- Speck, T. & Rowe, N. P. 2001 Plant architecture. In *Palaeobiology II* (ed. D. E. G. Briggs & P. R. Crowther), pp. 383–388. London: Blackwell Science.
- Speck, T. & Schmitt, M. (unter Mitarbeit von E.-M. Stahmer, G. Uhl, J. Lange & A. Parnesar) 1992 Tabellen. In *Biologie im Überblick, Lexikon der Biologie*, vol. 10 (ed. M. Schmitt), pp. 187–328. Freiburg: Herder Verlag.
- Speck, T. & Vogel-lehner, D. 1988 Biophysical examinations of the bending stability of various stele types and the upright axes of early ‘vascular’ land plants. *Botanica Acta* **101**, 262–268.

- Speck, T. & Vogellehner, D. 1994 Devonische Landpflanzen mit und ohne hypodermales Sterom—Eine biomechanische Analyse mit Überlegungen zur Frühevolution des Leit- und Festigungssystems. *Palaeontographica B* **233**, 157–227.
- Speck, T., Spatz, H.-C. & Vogellehner, D. 1990 Contribution to the biomechanics of plants. I. Stabilities of plant stems with strengthening elements of different cross-sections against weight and wind forces. *Botanica Acta* **103**, 111–122.
- Speck, T., Rowe, N. P., Brüchert, F., Haberer, W., Gallenmüller, F. & Spatz, H.-C. 1996 How plants adjust the 'material properties' of their stems according to differing mechanical constraints during growth—an example of smart design in nature. In *Bioengineering—PD*, vol. 77 (ed. A. E. Engin), pp. 233–241. *Proc. 1996 Engineering Systems Design and Analysis Conf.*, vol. 5, ASME.
- Speck, T., Speck, O., Emanns, A. & Spatz, H.-C. 1998 Biomechanics and functional anatomy of hollow stemmed sphenopsids: III. *Equisetum hyemale*. *Botanica Acta* **111**, 366–376.
- Stephens, R. C. 1970 *Strength of materials. Theory and examples*, reprint edn 1994. London: Arnold.
- Taylor, T. N. & Taylor, E. L. 1993 *The biology and evolution of fossil plants*. Englewood Cliffs, NJ: Prentice-Hall.
- Vincent, J. F. V. 1992 *Biomechanics—material: a practical approach*. Oxford: IRL Press at Oxford University Press.
- Wainwright, S. A., Biggs, W. D., Currey, J. D. & Gosline, J. M. 1976 *Mechanical design in organisms*. London: Arnold.
- Young, W. C. 1989 *Roark's formulas for stress & strain*, 6th edn. New York: McGraw-Hill.